Hydrogen Atom Formation in the Photolysis of Acetone at 193 nm†

Kenshi Takahashi,* Tomoki Nakayama, and Yutaka Matsumi

Solar-Terrestrial Environment Laboratory and Graduate School of Science, Nagoya University, 3-13 Honohara, Toyokawa, Aichi, 442-8507, Japan

Yoshihiro Osamura

Department of Chemistry, Rikkyo University, 3-34-1 Nishi-ikebukuro, Toshima-ku, Tokyo, 171-8501, Japan

Received: February 15, 2004; In Final Form: March 19, 2004

An experimental and theoretical study of the formation of hydrogen atom in the photolysis of acetone at 193 nm is reported. The H atom photofragments are detected by the technique of vacuum ultraviolet laser-induced fluorescence (VUV-LIF) spectroscopy at 121.6 nm. The quantum yield for H atom formation from acetone photolysis at 193 nm is determined to be 0.039 ± 0.006. The Doppler profiles of the H atom photofragments are measured by scanning the probe laser wavelength around the resonance frequency of the H atom at 121.6 nm. The nascent kinetic energy distribution of the H atom fragments is found to be characterized by a Maxwell−Boltzmann function with the temperature of 5000 K. The spatially isotropic recoil distribution in the H atom photofragmentation is observed. The potential energy surfaces for the H atom formation processes from acetone photolysis are examined using molecular orbital calculation methods. Atmospheric implications of the present result are briefly discussed.

Introduction

Acetone is the simplest ketone, and its primary photochemical process following ultraviolet excitation has been an important subject of photochemistry. The first absorption band in acetone centered at ∼270 nm corresponds to a $\pi^* \leftarrow$ n ($S_1 \leftarrow S_0$) transition, and the second absorption band ($S_2 \leftarrow S_0$), which results from a 3s ← n Rydberg excitation, starts at around 196 nm.[1−4] The α-cleavage process in the UV photolysis of acetone, which is known as Norrish type-I reaction, has been extensively studied:

$$CH_3COCH_3 \rightarrow 2CH_3 + CO \qquad \Delta H_f(298) = 95.5 \text{ kcal mol}^{-1} \quad (1)$$

$$\rightarrow CH_3CO + CH_3 \qquad \Delta H_f(298) = 84.5 \text{ kcal mol}^{-1} \quad (2)$$

The values of the standard heat of formation were calculated from the data reported by Sander et al.[5] Many experimental studies on the Norrish type-I reaction have been carried out to elucidate the dissociation dynamics of acetone in the ultraviolet region.[6−16] There has been great interest in the potential energy surfaces (PESs) of the excited states of acetone, and many theoretical studies have also been published on the reaction pathways of the Norrish type-I reaction.[14,17−22] For example, several mechanisms for channel 1 following the 193 nm excitation of acetone, which include internal conversion (IC) from the S_2 state to the S_1 state, have been proposed and still remain controversial. Lightfoot et al.[23] showed that both channels 1 and 2 account for >95% of the primary photolysis products from the 193 nm photolysis of acetone, using end product analysis and time-resolved absorption spectrometry techniques. They suggested that the dissociation into two channels of $H + CH_2COCH_3$ and $CH_4 + CH_2CO$ occurs with minor yields.

$$CH_3COCH_3 \rightarrow CH_3COCH_2 + H \qquad \Delta H_f(298) = 95.7 \text{ kcal mol}^{-1} \quad (3)$$

$$\rightarrow CH_4 + CH_2CO \qquad \Delta H_f(298) = 23.0 \text{ kcal mol}^{-1} \quad (4)$$

The enthalpy data were taken from Sander et al.[5] for H, CH_4, and CH_2CO, and from Bouchoux et al.[24] and Espinosa-García et al.[25] for CH_3COCH_2. Washida et al.[26] observed the production of $CH_3COCH_2(X^2A'')$ from acetone photolysis at 193 nm using the LIF detection for the B − X electronic transition of CH_3COCH_2 fragments, which implies the existence of the C−H bond scission process.

Most of the previous experimental and theoretical studies on the 193 nm photolysis of acetone have thus paid attention to channel 1, and no detailed study has been reported on the other channels. In this paper, we report on the experimental and theoretical study of hydrogen atom formation from the photolysis of acetone at 193 nm using vacuum UV laser-induced fluorescence spectroscopy (VUV-LIF) and quantum chemical calculations. The quantum yield for H atom formation is determined experimentally, in which HCl photolysis is used as a reference. We have explored the potential energy surfaces (PES) for the elimination process of the H atom from acetone photolysis in terms of density functional and ab initio molecular orbital calculations.

Experimental Section

The experimental arrangements and procedures for the VUV-LIF spectroscopic study of the photodissociation of acetone are

† Part of the special issue "Richard Bersohn Memorial Issue".

* Corresponding author. Fax: +81-533-89-5593.

10.1021/jp049320l CCC: $27.50
Published on Web 05/11/2004

essentially the same as those in our previous studies.[27,28] The photolysis radiation at 193 nm was generated using an excimer laser operating at 10 Hz repetition rate (Lambda Physik, Compex 102). The H atom photoproduct was detected by VUV-LIF using the $2p^2P_{1/2} - 1s^2S_0$ transition at 121.6 nm (Lyman-α). The necessary VUV radiation was generated by two-photon resonant four-wave difference frequency mixing in Kr gas,[29] using two tunable dye lasers (Lambda Physik, FL3002 and Scanmate 2E) pumped simultaneously by a XeCl excimer laser (Lambda Physik, COMPex 201). The output of one dye laser was frequency-doubled using a β-BaB_2O_4 crystal to generate UV light at 212.56 nm, which is two-photon resonant with the $5p[^1/_2]_0 - {}^1S_0$ transition of Kr. The second dye laser generated ~845 nm light. Typical intensities were 0.3 and 2 mJ/pulse for the ω_1 and ω_2 lasers, respectively.

The laser beams for the four-wave mixing were collinearly overlapped with a dichroic mirror and focused ($f = 200$ mm) into a stainless steel cell containing Kr gas. The typical pressure of Kr was 13 Torr. The resultant VUV radiation passed through a LiF window into the reaction chamber where it crossed at right angles with the photolysis laser beam. Another LiF window mounted in the chamber beyond the photodissociation region reflected part of the probe laser pulse toward a nitric oxide (NO)-containing cell. The photoionization current from NO gas was monitored to obtain the relative intensity variation of the VUV radiation. The typical NO gas pressure was 2 Torr. The delay time between the photolysis and probe laser pulses was controlled by a pulse generator (Stanford Research, DG535) and typically was set at 80 ns (but could be extended to as long as 25 μs) with a jitter of <10 ns.

The VUV-LIF of the H atom was detected along the vertical axis, orthogonal to propagation direction of both the VUV probe and photodissociation laser beams, using a solar blind photomultiplier tube (EMR, 541J-08-17) equipped with a LiF window and a KBr photocathode sensitive only to radiation in the wavelength range of 105−150 nm. A band-pass filter was installed (Acton Research, Model 122-VN, $\lambda = 122$ nm, $\Delta\lambda = 12$ nm). The output of the photomultiplier was preamplified and averaged over 10 laser pulses using a gated integrator (Stanford Research, SR-250).

The chamber is evacuated by a rotary pump (Alcatel 2520) through a liquid N_2 trap; a capacitance manometer (MKS, Baratron 220) was used to measure the sample gas pressure in the chamber. The sample gas of acetone (purity > 99.5%, Kanto Chemical Co.) was used after being degassed by freeze−pump−thaw cycles. Both helium (>99.99%) and argon (>99.999%) were used without further purification.

Computational Procedure

We have applied the hybrid density functional B3LYP method[30,31] with the 6-311G(d,p) basis set[32] to calculate the potential energy surfaces of the ground (S_0) and lowest triplet (T_1) states of acetone. We have calculated the molecular geometries of the transition states for the C−C and C−H bond scissions of acetone and its fragment caused by photodissociation. The structures on the potential energy surfaces were confirmed to be energy minima or transition states by vibrational analyses. In order to refine the relative energies on the potential energy surfaces, we have utilized the coupled cluster CCSD(T) method[33,34] with Dunning's augmented correlation consistent polarized valence triple-ζ basis set (aug-cc-pVTZ)[35,36] at the geometries obtained with the B3LYP method. The relative energies presented in this paper are corrected by the zero-point vibrational energy obtained with the B3LYP method without scaling. All computations were carried out using the Gaussian 98 program suite.[37]

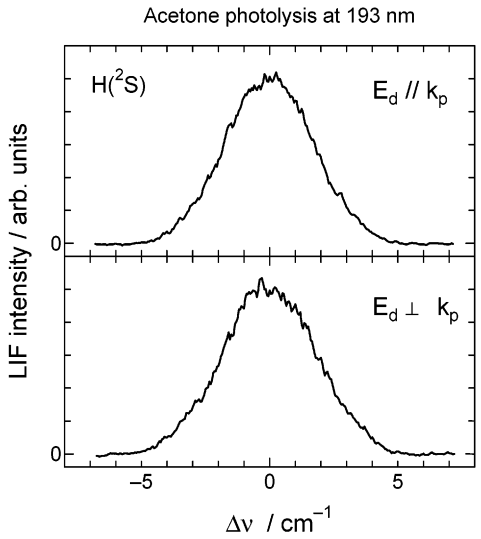

Figure 1. The VUV-LIF Doppler profiles of nascent H atoms produced in the 193 nm photolysis of acetone, in which the probe laser frequency was scanned around the resonant $2p^2P_{1/2} - 1s^2S_0$ transition at 121.6 nm. $\mathbf{E}_d \perp \mathbf{k}_p$ and $\mathbf{E}_d \| \mathbf{k}_p$ imply that the directions of the electronic vector of the linearly polarized dissociation laser light ($\mathbf{E}_d$) are perpendicular and parallel to the propagation directions of the probe laser beam ($\mathbf{k}_p$), respectively. The time delay between the dissociation and probe laser pulses was 80 ns, and the acetone pressure in the reaction cell was 10 mTorr without any buffer gas.

There was a computational difficulty in order to describe the H elimination on the S_1 state so that the relative energies were properly evaluated, because all six C−H bonds of acetone have to be treated equivalently at the reactant stage even if one of the C−H bonds is breaking. There are several simple ways to explore the lowest excited singlet state based on a single reference electron configuration, and we have tried to carry out CIS[38] and TD-DFT[39] methods in order to draw the potential curve along one of the C−H bond distances of acetone on the S_1 surface. However, all calculations lead to the uphill potential toward the H elimination pathway due to the incorrect description of the reference Hartree−Fock orbitals of the ground state and fail to locate the transition state of the C−H bond scission on the S_1 state. Since the calculation of the potential energy surface of the S_1 state along the C−H bond dissociation cannot be well described unless one uses a large number of active space (almost full valence space) in the multiconfigurational approach, we have only treated the lowest triplet state as well as the ground state to investigate the H atom elimination processes of acetone in the present study.

Results

1. Doppler Profiles for Nascent H Atom Fragments. Figure 1 shows the Doppler profiles of the H atoms from the photodissociation of acetone at 193 nm, in which the H atom fragments were directly detected by the LIF technique. The VUV probe laser was scanned across the resonant frequency for the $2p^2P_{1/2} - 1s^2S_0$ electronic transition at 121.6 nm. The delay time between the dissociation and probe laser pulses was fixed at 80 ns. The pressure of acetone was 10 mTorr, and no buffer gas was added in the reaction chamber. For the measurement of the polarization effect on the Doppler profiles, two different configurations, $\mathbf{E}_d \| \mathbf{k}_p$ and $\mathbf{E}_d \perp \mathbf{k}_p$, were used, where $\mathbf{E}_d$ is the polarization vector of the dissociation laser and $\mathbf{k}_p$ is the propagation direction of the probe laser. The 193 nm laser

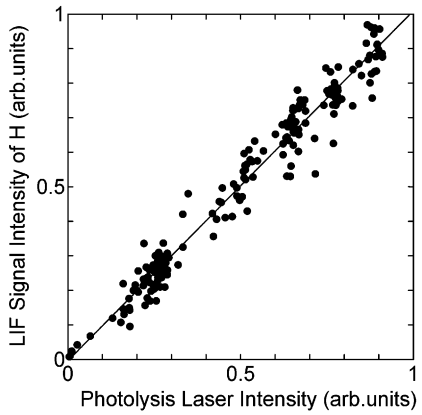

Figure 2. H atom LIF signal intensity vs 193 nm laser intensity. Acetone molecules (10 mTorr) were photolyzed at 193 nm, and the H atoms produced were detected directly using the VUV-LIF technique at 121.6 nm. The delay time between the pump-and-probe laser pulses was 80 ns. The straight line indicates the result of the linear least-squares fit analysis of the data measured.

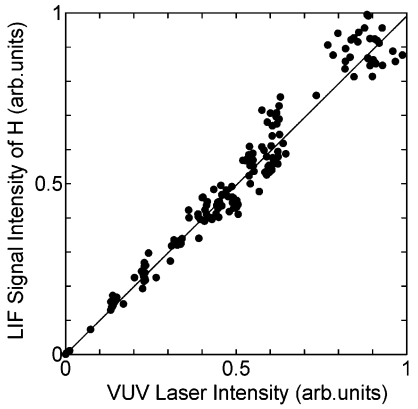

Figure 3. H atom LIF signal intensity vs probe laser intensity. Acetone molecules (10 mTorr) were photolyzed at 193 nm, and the H atoms produced were detected directly using the VUV-LIF technique at 121.6 nm. The delay time between the pump-and-probe laser pulses was 80 ns. The intensity of the VUV laser was varied by changing the Kr gas pressure in the frequency conversion cell between 0 and 20 Torr, while keeping the output power of the 193 nm laser constant.

light was polarized by a pile-of-plate polarizer. The Doppler profiles of the nascent H photofragments have much larger widths than the probe laser line width. As shown in Figure 1, the Doppler spectra taken under the two optical configurations show no difference in their spectral shapes, which indicates that the velocities of the H atom fragments have an isotropic angular distribution. The probe laser line width was estimated to be 0.7 cm^{-1} full width at half-maximum (fwhm) with a Gaussian shape. This value was determined by a simulation procedure so that the Doppler profile of the completely thermalized H atoms at a delay time of 20 μs in the presence of 1.7 Torr of Ar was reproduced by the Maxwell−Boltzmann distribution at room temperature.

Checks were made to ensure that the LIF signal scaled linearly with the intensity of the photodissociation laser pulse as shown in Figure 2. We also found that no detectable H atom was observed when the 193 nm laser was not operating. These results indicate that multiphoton absorption processes or photodissociation of parent molecules at the probe laser wavelength were safely ignored in this work. Next, we measured the LIF intensity as a function of the VUV probe laser intensity, where the probe laser intensity was varied by changing the pressure of Kr gas. Figure 3 shows a linear power dependence of the LIF signal on the VUV probe laser intensity. This indicates that the H atom formation from the secondary Lyman-α dissociation of primary photoproducts can be ignored under our experimental conditions.

The Doppler spectra reflect the distributions of the projection of the velocity along the direction of the probe laser, and they are broadened by the probe laser line width.[40] We used a direct method with least-squares fitting of experimental Doppler profiles in order to extract speed distributions of the H atoms from acetone. Since the detailed procedure and mathematical expressions were described previously,[41] only the principle of the procedure is briefly presented here. Experimental Doppler profiles are divided into equally spaced frequency points, ω_k, ($k = 1 - m$). Then, a magic angle spectrum, $Y^+_k(k = 1 - m)$, is generated by summing the parallel ($\mathbf{E}_d \| \mathbf{k}_p$) and the perpendicular ($\mathbf{E}_d \perp \mathbf{k}_p$) components in a one-to-two ratio.[42] This spectrum reflects a speed distribution free from the angular anisotropy. In the following discussion, we assume that a speed distribution is expressed by a finite set of speed components, v_i ($i = 1 - n$), which are equally spaced with weights of f_i. Thus, a theoretical Doppler profile, $S(k, i)$, is calculated for the magic angle alignment with convolution of the laser line width. Then,

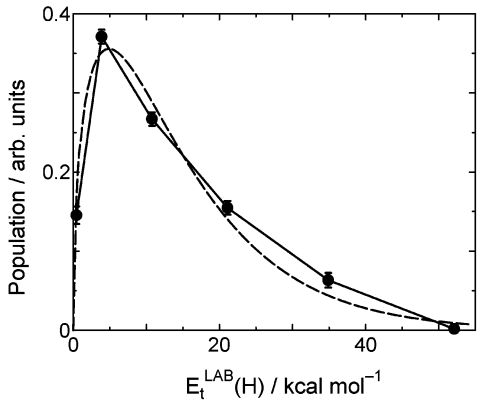

Figure 4. Kinetic energy release spectrum of the nascent H atoms produced in the 193 nm photolysis of acetone in the laboratory flame, as revealed from the analysis of the Doppler profiles shown in Figure 1. The dashed curve indicates the Boltzmann distribution function with the temperature of 5000 K.

we apply a singular-value decomposition method with least-squares fitting in order to determine the coefficient a_i of the v_i component in the experimental sum spectrum, $a_i = v_i^2 f_i$.

We calculated the velocity distributions of the H atoms from the Doppler spectra shown in Figure 1. The speed distributions are obtained at the speed points, v_i ($i = 1-6$) with an interval of 3797 m s^{-1} using a least-squares fitting method. For the analysis, the spectra recorded under the same experimental conditions were averaged over eight runs to increase signal-to-noise ratios, and then the $\mathbf{E}_d \| \mathbf{k}_p$ spectrum and twice the $\mathbf{E}_d \perp \mathbf{k}_p$ spectrum were summed to obtain the magic angle spectrum. Thus, the velocity distribution was calculated, and it was converted to the translational energy distribution by using its appropriate Jacobian. It should be noted that the Doppler profiles shown in Figure 1 clearly indicate the isotropic angular distribution in the nascent H atom fragments from acetone.

Figure 4 shows the translational energy distributions of the nascent H atoms produced from the 193 nm photolysis of acetone. The average translational energy release of the H atom fragments in the laboratory (LAB) flame, $\langle E_t^{LAB}(H) \rangle$, was obtained to be 14.3 kcal mol^{-1}. We found that the translational energy distribution is characterized by a Maxwell−Boltzmann function with the temperature of 5000 K as depicted by the dashed curve in Figure 4.

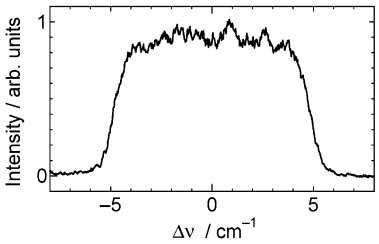

Figure 5. Fluorescence excitation spectrum of the H atoms produced in the 193 nm photolysis of HCl, in which the H atoms were detected with the VUV-LIF method at 121.6 nm. The time delay between the dissociation and probe laser pulses was 120 ns, and the acetone pressure in the reaction cell was 55 mTorr with 357 mTorr of Ar.

The Gaussian line shape of the Doppler spectra shown in Figure 1 is consistent with an isotropic Maxwellian distribution of velocities. The relationship between the fwhm (full width at half-maximum) of the Doppler spectrum $\Delta\nu$, the center frequency ν_0, and the temperature characterizing the Boltzmann translational energy distribution T is given by[43]

$$T = \left(\frac{\Delta\nu}{2\nu_0}\right)^2 \frac{mc^2}{2k_B \ln 2} \quad (5)$$

in which k_B is the Boltzmann constant, m is the mass of the fragment, and c is the speed of light. The average kinetic energy $\langle E_t^{LAB}(H)\rangle = (^3/_2)kT$ calculated from eq 5 is 14.8 kcal mol^{-1}, which is consistent with that derived from the singular-value decomposition analysis of the Doppler spectra as described above.

2. Quantum Yield for H Atom Formation. This paper presents the first direct detection of H atom from acetone photolysis at 193 nm. The quantum yield for H atom formation in the 193 nm photolysis, Φ_H, was determined. The sample gases of acetone/Ar (3.9%) and HCl/Ar (13.5%) were alternatively photolyzed with the unpolarized 193 nm laser light, and the H atom production was detected by the VUV-LIF technique. Typical total pressures were 350−450 and 340−500 mTorr for acetone/Ar and HCl/Ar, respectively. A typical spectrum of the H atom from HCl photolysis is shown in Figure 5, in which the translational energy of the H atom produced is partly relaxed under our experimental conditions. The time delay between the dissociation and probe laser pulses was 120 ns. The dissociation laser intensity varies little (<5%) through the measurements. Since the 193 nm photolysis of HCl generates H atoms with a quantum yield of unity, the Φ_H value was obtained by the following equation:

$$\Phi_H = \frac{S_{acetone}\sigma_{HCl}[HCl]}{S_{HCl}\sigma_{acetone}[acetone]} \times 1 \quad (6)$$

where [acetone] and [HCl] are the concentrations of acetone and HCl, respectively; $\sigma_{acetone}$ and σ_{HCl} are the absorption cross sections for acetone and HCl at 193 nm, respectively. Because the acetone absorption shows a very steep increase around 193 nm,[1,2] it was difficult to obtain the cross section value at 193 nm from the spectra presented in published papers. In this work, we measured the cross section $\sigma_{acetone}$ at the 193 nm ArF laser wavelength. Figure 6 shows a Beer−Lambert plot of the 193 nm absorption of acetone. The cross section value obtained in this work was 3.71×10^{-18} cm^2 molecule^{-1} and was in good agreement with the visual inspection of the reported spectrum.[1] For σ_{HCl}, the reported value (8.69×10^{-20} cm^2 molecule^{-1})[5,44] was used. $S_{acetone}$ and S_{HCl} were obtained by integrating the measured Doppler profiles of the H atoms, in which both spectra were corrected for the relative intensity variation of the VUV probe laser. Several experimental runs were performed to record the fluorescence excitation spectra. Thus, $\Phi_H = 0.039 \pm 0.006$ was obtained, where the quoted error was the 2σ statistical uncertainty of the experimental data.

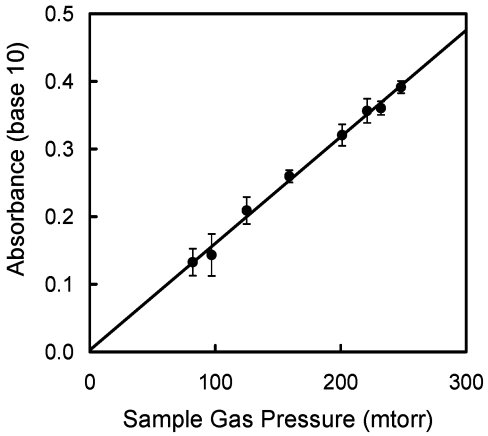

Figure 6. Beer−Lambert plot for photoabsorption of acetone at 193.3 nm. The straight line is the result from the linear least-squares fit analysis of the absorbance measurements.

3. Potential Energy Surfaces of Acetone. Figure 7 shows the schematic PESs of the S_0 and T_1 states of acetone along the C−C and C−H dissociation pathways. Both pathways have reverse energy barriers on the T_1 and S_1 surfaces but not in the ground state S_0. Figure 8 illustrates the molecular geometries of the energy minima and transition states presented in Figure 7. Ground state acetone has C_{2v} symmetry, while the T_1 state of acetone has an energy minimum with C_s symmetry.

The bond dissociation energy 91.3 kcal mol^{-1} for channel 2 seems to be somewhat overestimated in comparison with the value of 84.5 kcal mol^{-1} calculated from the enthalpy data presented by Sander et al.[5] The energy of the transition state TSa of the C−C bond cleavage on the T_1 surface is calculated to be 14.1 kcal mol^{-1} at the CCSD(T) level of theory. This value is in reasonable agreement with the previous calculation but not with CASSCF level of theory.[14,15,16,21] The transition state TSc is the second C−C bond cleavage from CH_3CO to $CH_3 + CO$, and its energy barrier of 15.2 kcal mol^{-1} obtained in the present study is slightly small compared to the previous theoretically and experimentally estimated values.[9,14,15,21,22] Considering these facts, the energetics concerned with the C−H dissociation may involve errors of a few kcal mol^{-1} in its evaluation.

The dissociation energy to acetonyl radical CH_3COCH_2 from acetone (channel 3) is calculated to be 104.6 kcal mol^{-1} which is 13.3 kcal mol^{-1} higher in energy than the C−C bond cleavage. The structure of the ground state of the acetonyl radical has C_s symmetry, and its electronic state is $^2A''$. This CH_3COCH_2 ($^2A''$) is accessible from both the S_0 and T_1 states. The structure of the acetonyl radical is similar to that of acetone in the ground state. Since the radical center locates at the π-orbital of the terminal carbon atom, the C═O bond is slightly lengthened due to the π-conjugation between the C═O double bond and the radical orbital. The structure of the transition state TSb indicates that the elimination of the H atom is located almost above the C−C−O plane, and strong π-conjugation at the C−C−O moiety can be observed, where both C−O and C−C distances (1.296 Å and 1.376 Å, respectively) are shortened from the equilibrium structure of the T_1 state. Although this structure of TSb seems to be close to the structure of the excited state of the acetonyl radical CH_3COCH_2 ($^2A'$), the potential energy surface correlates

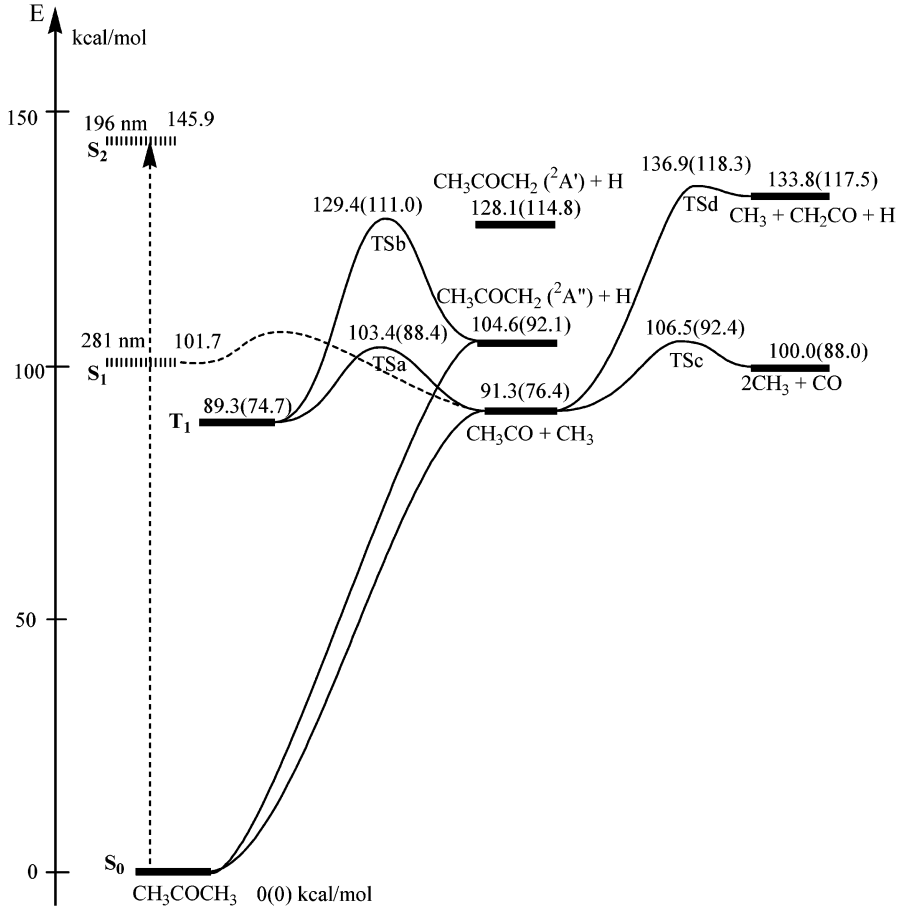

Figure 7. Schematic potential energy surfaces of photodissociation processes involving C−C and C−H bond dissociations of acetone in the ground (S_0) and lowest triplet (T_1) states calculated with the CCSD(T)/aug-cc-pVTZ level of theory. The relative energies shown in parentheses are the values obtained with the B3LYP/6-311G(d,p) level of theory.

to the ground state ($^2A''$) of the acetonyl radical. Noticing that the energy of the transition state TSb in the T_1 state is almost identical to the energy of the excited state of the acetonyl radical (128.1 kcal mol^{-1}), we would suspect that large mixing in the electronic structures is evolving at the region of the C−H bond dissociation in the excited states.

The adiabatic excitation energy of the acetonyl radical from the ground $^2A''$ state to the first exited $^2A'$ state is calculated to be 23.5 kcal mol^{-1} which agrees well with the value reported by Alconcel et al.[45] They measured the photoelectron spectra of acetone enolate at 355 nm and determined the separation energy between the X and A electronic states of acetonyl to be 23.2 ± 0.46 kcal mol^{-1}.

Discussion

In the present study, the H atom formation from the 193 nm photolysis of acetone has been detected using the VUV-LIF method. The kinetic energy release spectrum shown in Figure 4 suggests that the H atom fragments are translationally excited due to partitioning of the available energy. The available energy is given by $h\nu - D_0$, in which $h\nu$ is photon energy of the dissociation laser light (147.9 kcal mol^{-1}) and D_0 is the bond dissociation energy to produce the H atom. We performed B3LYP calculations to estimate the energetics for two H atoms production processes from one acetone molecule. The energetics for the products of 2H + $CH_2COCH_2(^3B_1)$ and 2H + CH_3-$COCH(^3A'')$ were 201.9 and 198.1 kcal mol^{-1} relative to ground state acetone, respectively. Therefore, we can exclude the possibility of the elimination of two H atoms in the photodissociation of acetone at 193 nm. Because the mass of the H atom is light and that of the counterpart is heavy, the translational energy distribution of H atoms in the LAB frame in Figure 4 almost coincides with the distribution of the kinetic energy release in the center-of-mass (CM) frame for the H atom elimination process in the photolysis of acetone.

The available energy for channel 3 is 52.2 (= 147.9−95.7) kcal mol^{-1}, which is very close to the maximum kinetic energy observed for the H atoms shown in Figure 4. Therefore, it is probable that channel 3 is responsible for the H atom formation process. This mechanism is consistent with the identification of acetonyl radical formation from the 193 nm photolysis of acetone by the LIF spectroscopy technique.[26]

The quantum yield for H atom formation from acetone photolysis at 193 nm has been determined to be $\Phi_H = 0.039 \pm 0.006$ in the present study. The very small Φ_H value is consistent with the report that the Norrish type-I reaction via channels 1 and 2 proceeds predominantly at 193 nm.[23] The Φ_H value obtained in this study is close to the channel 3 fractional yield (3%) determined by Lightfoot et al.[23] through the products analysis. They observed methyl ethyl ketone produced through the reaction of methyl and acetonyl radicals by gas chromatography. Those radicals are the primary photochemical products from channels 1 and 3.

We examine the possibility of H atom formation from the decomposition of the primary photodissociation products and three-body photodissociation. The formation of two H atoms in the photolysis of acetone at 193 nm is energetically impossible as described above. The H atom elimination channel which is

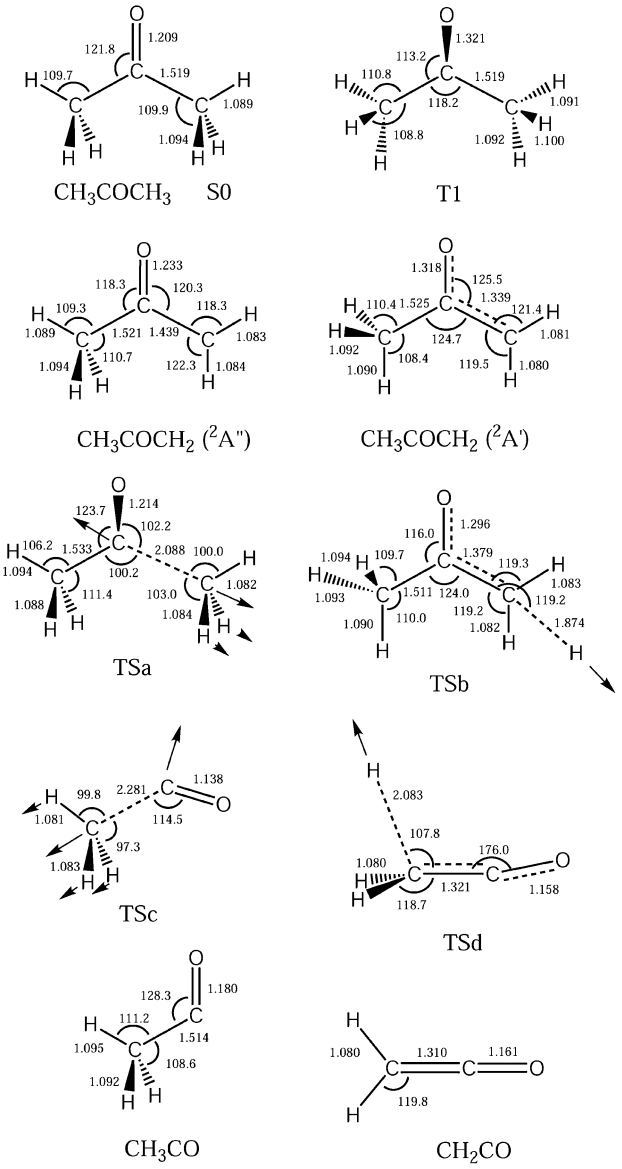

Figure 8. Molecular geometries at the stationary points shown in Figure 7. Arrows indicate the imaginary frequency modes at the transition states. Bond distances and bond angles are shown in units of angstroms and degrees, respectively.

energetically possible is

$$CH_3COCH_3 \rightarrow CH_3 + CH_2CO + H \qquad \Delta H_f(298) = 128 \text{ kcal mol}^{-1}\ ^5 \quad (7)$$

The energy of transition state TSd is calculated to be 45.6 kcal mol^{-1} relative to the acetyl radical, and this energy is only 3.1 kcal mol^{-1} above the energy of products $CH_2CO + H$, as depicted in Figure 7. However, the kinetic energy release spectrum in Figure 4 indicates that the H atom formation from channel 7 cannot account for all of the H atoms observed, since the available energy is 19.9 kcal mol^{-1} for this channel.

We also examine the possibility to produce electronically excited acetonyl radical:

$$CH_3COCH_3 \rightarrow CH_3COCH_2(A^2A') + H \qquad \Delta H_f(298) = 119 \text{ kcal mol}^{-1} \quad (8)$$

The electronic energy of $CH_3COCH_2(A^2A')$ estimated from our ab initio calculation is in good agreement with the recent experimental report.[45] Taking the energy into account, the available energy for channel 8 in the 193 nm photolysis of acetone is calculated to be 28.9 kcal mol^{-1}. The kinetic energy distribution in Figure 4 indicates that channel 8 cannot account for the H atom formation with the translational energy up to 50 kcal mol^{-1}.

On the basis of the considerations described above, it is probable that channel 3 is responsible for the H atom formation in the photodissociation of acetone at 193 nm. While there is no intrinsic barrier to dissociation to $CH_3COCH_2 + H$ on the S_0 surface, the transition state TSb on the triplet manifold has a reverse barrier of 24.8 kcal mol^{-1} as shown in Figure 7. When the exit channel barrier exists in the reaction coordinate, it is generally known that the energy of the reverse barrier is mostly transformed into the product translation. For instance, the dynamics of the C−C bond scission (channels 1 and 2) on the T_1 state is characterized by the existence of an exit barrier along the dissociation coordinate.[9,18,22] The kinetic energy release spectrum for the H atom formation process (Figure 4) peaks at about 5 kcal/mol and has significant populations up to the available energy with an average kinetic energy of $\langle E_t^{CM} \rangle \approx \langle E_t^{LAB}(H) \rangle = 14.3$ kcal mol^{-1}. The reverse barrier height along TSb on the T_1 surface is larger than that expected from the kinetic energy release spectrum. A plausible mechanism of the H atom elimination is as follows: after 193 nm excitation the initially prepared acetone in the S_2 state changes the surface to the S_1 state, which is followed by the internal conversion (IC) to the S_0 state on which acetone dissociates to yield H atom. The formation of H atoms from hot ground state molecules following the UV excitation of aromatic molecules has been reported by Bersohn and co-workers.[46,47] They derived the kinetic energy distributions from the Gaussian Doppler broadening of the excitation spectra of H atom.

Owrutsky and Baronavski[13] studied the photodissociation dynamics of the S_2 state of acetone by means of femtosecond pump-and-probe techniques. They reported the two time constants of 4.7 and 3.1 ps from the parent and the fragment ion signals, respectively. Zhong et al.[21] reported similar values of lifetimes (2.5−2.9 ps) of the various ketones in their S_2 state following photoexcitation at 195 nm. As summarized in the paper reported by Sølling et al.,[15] a relatively slow $S_2 \rightarrow S_1$ internal conversion (IC) process (~3 ps) is characteristic in the photochemical process of acetone excited onto the S_2 state. The relatively long dissociation lifetime provides a straightforward explanation for the isotropic angular distribution of the H atom fragments observed in the present study. North et al.[9] photodissociated the molecular beam of acetone at 193 nm and measured the product state distribution of CH_3 radicals. They observed an isotropic recoil distribution of the CH_3 radicals, and the result is rationalized by rotational motion of the parent molecule prior to dissociation because of the relatively long dissociation lifetime.

It would be interesting to comment on the atmospheric significance of H atom production from acetone photolysis, because acetone is a widespread trace constituent of the atmosphere and its oxidation is an important source of HO_x radicals in the upper troposphere and lowermost stratosphere.[48] Wohlfrom et al.[49] observed acetone with mixing ratios ranging from 200 to 2000 pptv in the free troposphere and 100 to 200 pptv in the lowermost stratosphere. Primary HO_x production is dominated by the $O(^1D) + H_2O$ reaction when the mixing ratio of H_2O is over 100 ppmv and by photolysis of acetone and other HO_x precursors under drier conditions. Atmospheric

modeling has shown the major sink of acetone to be the oxidation that is initiated either by photolysis (64%) or by reaction with OH radicals (24%).[50] The former generates methyl and acetyl radicals through channel 2 dominantly, and the radicals are converted to HO_x by some chain reactions. The atmospheric HO_x production yield from acetone photolysis is a function of NO_x concentration. For example, the HO_x yield from acetone photolysis ranges from 2 to 3 for the principally northern midlatitude conditions sampled by the aircraft missions.[48]

The new finding in this work is the H atom production channel in the UV photolysis of acetone. The H atom produced is quickly converted to HO_x in the atmosphere by the recombination reaction with O_2, and thus the H atom formation in the acetone photolysis can be a direct source of HO_x even without NO_x. We roughly estimated the H atom production efficiency from acetone photolysis in the atmosphere at 10 km, using the available solar spectrum, acetone absorption spectrum, and the Φ_H value. The acetone absorption spectrum is taken from the report by Lake and Harrison.[1] Quantum yields for the photodissociation of acetone around 280−320 nm were calculated with the formulation reported by Gierczak et al.[51] At 10 km, the solar photon flux around 200 nm is very small. The photolysis of acetone dominates above 280 nm, and the photodissociation rate of acetone around the 200 nm region is less than 1% of the total rate between 190 and 340 nm at 10 km. The H atom quantum yield from acetone photolysis at 193 nm is 0.039 ± 0.006, as determined in this study. Assuming that the photolytic H atom formation occurs around 200 nm ($S_2 \leftarrow S_0$ excitation), the H atom production efficiency in the total acetone photolysis rate between 190 and 340 nm is less than 3.9×10^{-4}. This result indicates that the photolytic H atom formation from acetone around 200 nm is not a significant source of HO_x radicals in the lowermost stratospheric and tropospheric photooxidation of acetone.

Acknowledgment. This work was supported by a Grant-in-Aid from the Ministry of Education, Culture, Sports, Science and Technology, Japan. The authors thank the computer center of the Institute for Molecular Science, Japan for generous access to computational resources. The authors thank Dr. Satoshi Inomata of the National Institute for Environmental Studies for helpful comments.

References and Notes

(1) Lake, J. S.; Harrison, A. J. *J. Chem. Phys.* **1959**, *30*, 361.
(2) Barnes, E. E.; Simpson, W. T. *J. Chem. Phys.* **1961**, *39*, 670.
(3) Martinez, R. D.; Buitrago, A. A.; Howell, N. W.; Hearn, C. H.; Jones, J. A. *Atmos. Environ.* **1992**, *26A*, 785.
(4) Yujing, M.; Mellouki, A. *J. Photochem. Photobiol.* **2000**, *A134*, 31.
(5) Sander, S. P.; Friedl, R. R.; Golden, D. M.; Kurylo, M. J.; Huie, R. E.; Orkin, V. L.; Moortgat, G. K.; Ravishankara, A. R.; Kolb, C. E.; Molina, M. J.; Finlayson-Pitts, B. J. *Chemical Kinetics and Photochemical Data for Use in Atmospheric Studies, Evaluation No. 14*; JPL Publication 02-25, 2003.
(6) Woodbridge, E. L.; Fletcher, T. R.; Leone, S. R. *J. Phys. Chem.* **1988**, *92*, 5387.
(7) Trentelman, K. A.; Kable, S. H.; Moss, D. B.; Houston, P. L. *J. Chem. Phys.* **1989**, *91*, 7498.
(8) Hall, G. E.; Bout, V.; Sears, T. J. *J. Chem. Phys.* **1991**, *94*, 4182.
(9) North, S. W.; Blank, D. A.; Gezelter, J. D.; Longfellow, C. A.; Lee, Y. T. *J. Chem. Phys.* **1995**, *102*, 4447.
(10) Hall, G. E.; Metzler, H. W.; Muckerman, J. T.; Preses, J. M.; Weston, R. E., Jr. *J. Chem. Phys.* **1995**, *102*, 6660.
(11) Kim, S. K.; Pedersen, S.; Zewail, A. H. *J. Chem. Phys.* **1995**, *103*, 477.
(12) Shibata, T.; Suzuki, T. *Chem. Phys. Lett.* **1996**, *262*, 115.
(13) Owrutsky, J. C.; Baronavski, A. P. *J. Chem. Phys.* **1998**, *108*, 6652.
(14) Diau, E. W.-G.; Kötting, C.; Zewail, A. H. *ChemPhysChem*. **2001**, *2*, 273.
(15) Sølling, T. I.; Diau, E. W.-G.; Kötting, C.; De Feyter, S.; Zewail, A. H. *ChemPhysChem*. **2002**, *3*, 79.
(16) Chen, W.-K.; Ho, J.-W.; Cheng, P.-Y. *Chem. Phys. Lett.* **2003**, *380*, 411.
(17) Setokuchi, O.; Matsuzawa, S.; Shimizu, Y. *Chem. Phys. Lett*. **1998**, *284*, 19.
(18) Sakurai, H.; Kato, S. *J. Mol. Struct. (THEOCHEM)* **1999**, *461*, 145.
(19) Liu, D.; Fang, W.-H.; Fu, X.-Y. *Chem. Phys. Lett.* **2000**, *325*, 86.
(20) Diau, E. W.-G.; Kötting, C.; Sølling, T. I.; Zewail, A. H. *ChemPhysChem.* **2002**, *3*, 57.
(21) Zhong, Q.; Steinhurst, D. A.; Baronavski, A. P.; Oerutsky, J. C. *Chem. Phys. Lett.* **2003**, *370*, 609.
(22) Martínez-Núñez, E.; Fernández-Ramos, A.; Cordeiro, M. N. D. S.; Vázquez, S. A.; Aoiz, F. J.; Bañares, L. *J. Chem. Phys.* **2003**, *119*, 10618.
(23) Lightfoot, P. D.; Kirwan, S. P.; Pilling, M. J. *J. Phys. Chem.* **1988**, *92*, 4938.
(24) Bouchoux, G.; Chamot-Rooke, J.; Leblanc, D.; Mourgues, P.; Sablier, M. *ChemPhysChem.* **2001**, *4*, 235.
(25) Espinosa-García, J.; Márquez, A.; Dóbé, S. *Chem. Phys. Lett.* **2003**, *373*, 350.
(26) Washida, N.; Inomata, S.; Furubayashi, M. *J. Phys. Chem.* **1998**, *A102*, 7924.
(27) Hitsuda, K.; Takahashi, K.; Matsumi, Y.; Wallington, T. J. *J. Phys. Chem.* **2001**, *A105*, 5131.
(28) Inagaki, Y.; Matsumi, Y.; Kawasaki, M. *Bull. Chem. Soc. Jpn.* **1993**, *66*, 3166.
(29) Marangos, J. P.; Shen, N.; Ma, H.; Hutchinson, M. H. R.; Cornerade, J. P. *J. Opt. Soc. Am.* **1990**, *B7*, 1254.
(30) Becke, A. D. *J. Chem. Phys.* **1993**, *98*, 5648.
(31) Lee, C.; Yang, W.; Parr, R. G. *Phys. Rev. B* **1988**, *37*, 785.
(32) Krishnan, R.; Binkley, J. S.; Seeger, R.; Pople, J. A. *J. Chem. Phys.* **1980**, *72*, 650.
(33) Cizek, J. *Adv. Chem. Phys.* **1969**, *14*, 35.
(34) Pople, J. A.; Head-Gordon, M.; Raghavachari, K. *J. Chem. Phys.* **1987**, *87*, 5968.
(35) Dunning, T. H., Jr. *J. Chem. Phys*. **1989**, *90*, 1007.
(36) Kendall, R. A.; Dunning, T. H.; Harrison, R. J. *J. Chem. Phys.* **1992**, *96*, 6796.
(37) Frisch, M. et al. *Gaussian 98*, revision A.11; Gaussian, Inc.: Pittsburgh, PA, 2002.
(38) Foresman, J. B.; Head-Godon, M.; Pople, J. A.; Frish, M. J. *J. Phys. Chem.* **1992**, *96*, 135.
(39) Stratmann, R. E.; Scuseria, G. E.; Frish, M. J. *J. Chem. Phys*. **1999**, *109*, 8218.
(40) Bersohn, R.; Lin, S. H. *Adv. Chem. Phys.* **1969**, *16*, 80.
(41) Matsumi, Y.; Shamsuddin, S. M.; Sato, Y.; Kawasaki, M. *J. Chem. Phys*. **1994**, *101*, 9610.
(42) Zare, R. N. *Angular Momentum*; Wiley-Interscience: New York, 1988.
(43) Zare, R. N.; Herschbach, D. R. *Proc. IEEE*. **1963**, *51*, 173.
(44) Goldfarb, L.; Schmoltner, A.-M.; Gilles, M. K.; Burkholder, J. B.; Ravishankara, A. R. *J. Phys. Chem.* **1997**, *A101*, 6658.
(45) Alconcel, L. S.; Deyerl, H.-J.; Continetti, R. E. *J. Am. Chem. Soc.* **2001**, *123*, 12675.
(46) Yi, W.; Chattopadhyay, A.; Bersohn, R. *J. Chem. Phys*. **1991**, *94*, 5994.
(47) Tsukiyama, K.; Bersohn, R. *J. Chem. Phys.* **1987**, *86*, 745.
(48) Jaeglé, L.; Jacob, D. J.; Brune, W. H.; Wennberg, P. O. *Atmos. Environ.* **2001**, *35*, 469.
(49) Wohlfrom, K.-H.; Hauler, T.; Arnold, F.; Singh, H. B. *Geophys. Res. Lett.* **1999**, *26*, 2849.
(50) Wollenhaupt, M.; Carl, S. A.; Horowitz, A.; Crowley, J. N. *J. Phys. Chem.* **2000**, *A104*, 2695.
(51) Gierczak, T.; Burkholder, J. B.; Bauerle, S.; Ravishankara, A. R. *Chem. Phys.* **1998**, *231*, 229.